In-Process Monitoring of Surface Roughness of Internal Channels Using

Zeqing Sun[1] , Peng Zuo[2], Mato Pavlovic[2], Yi Feng Ang[2],
and Zheng Fan[1(✉)]

[1] School of Mechanical and Aerospace Engineering,
Nanyang Technological University, 50 Nanyang Avenue,
Singapore 639798, Singapore
`zfan@ntu.edu.sg`
[2] Advanced Remanufacturing and Technology Centre (ARTC),
3 CleanTech Loop, #01/01, CleanTech Two, Singapore 637143, Singapore

Abstract. Additively manufactured (AM) parts generally have a higher surface roughness than parts manufactured using conventional methods. In most applications, a smooth surface finishing is preferred since rough surfaces are prone to corrosion attacks and fatigue crack incubation. Therefore, surface finishing is necessary to reduce the surface roughness of AM parts before they are used. The roughness of outer surfaces can be measured directly, using either contact stylus profilometer or non-contact optical microscope. However, there are still challenges to quantify the roughness of the internal surfaces using these conventional techniques of surface metrology. In this paper, we present a method to measure the roughness of internal channels by analyzing ultrasonic signals from the backwall reflection. A frequency-domain technique based on phase-screen approximation is used to reconstruct the root mean square (R_q) value from the ultrasonic signal scattered from the rough surfaces. Finite element simulations are developed to demonstrate the method, showing excellent accuracy when the R_q value is within 1/15 of the wavelength of the incident ultrasound. The method is then applied to monitor the surface roughness of the internal channels during the Abrasive Flow Machining (AFM) process. The reconstructed roughness value shows a clear and steady downward trend during the polishing process, quantitatively indicating the polishing rate. This demonstrates that such ultrasonic method can be used as a tool to provide feedback controls in the polishing process.

Keywords: Additive manufacturing · Roughness · Ultrasound · Online monitoring · Abrasive flow machining

1 Introduction

Compared with conventional methods to produce metallic components, additive manufacturing (AM) has advantages of excellent design freedom and wide range of selectable materials. However, additively manufactured parts generally have rough surfaces, and polishing is usually needed to meet functional requirements, and to reduce the risk of fatigue crack initiation [1, 2].

The complex geometry of AM parts, e.g., internal features, make inspection challenging since common measurement techniques such as stylus profiling, optical microscopy and confocal microscopy cannot access the internal surfaces. This work addresses the challenge to monitor the roughness of internal surface while they are being polished with techniques like Abrasive Flow Machining (AFM), with the roughness values (R_q) usually starting from 20–40 μm.

It is widely known that the ultrasonic waves are affected by the profile/finish of the surfaces they impinge on. There are two primary effects: rough surfaces attenuate the higher frequency components of a wave more that the lower frequencies, leading to a non-linear change in the frequency spectrum of the reflected wave; rough surfaces cause diffuse scattering of the wave leading to more ultrasonic energy being reflected at diffuse angles rather than at the specular angle. There are a number of ways to reconstruct the roughness value from ultrasonic signals. Amplitude based method can be used to estimate the roughness of a surface [3–8], as rougher surface would cause stronger attenuation of the interacting ultrasound. However, this method is affected by the variation of the coupling between the ultrasonic transducers and the target component. Furthermore, roughness information can also be extracted from the spectrum of a signal [9, 10] as the attenuation depends on the wavelength/roughness ratio. It is worth mentioning that angular-based techniques that utilize diffusive components can also be used to determine the roughness of a surface by measuring the ultrasound scattered into different directions [11–16]. However, they are less practical in this application due to limited space available to install monitoring sensors. In our work, a frequency domain method based on phase-screening approximation is applied to monitoring the surface roughness during a polishing process. Finite element studies as well as experiments are carried out to demonstrate the capability and the accuracy of the proposed method.

2   Methodology

2.1   Phase-Screen Approximation

The amount of reflection can be quantified using the phase-screen approximation: although roughness affects both the phase and the amplitude of the ultrasonic wave, the change in phase are dominant and therefore easier to be picked up [9, 17].

Using the phase-screen approximation, the amplitude of the reflection on a surface complying with Gaussian distribution is given by:

$$a(k) = a_0 \exp\left[-0.5R_q^2 k^2 (\cos\theta_i + \cos\theta_r)^2\right] \tag{1}$$

where a_0 is the reflected amplitude from a smooth surface, which is independent of wavenumber k. θ_i is the incident angle and θ_r is the reflected angle, with respect to the direction normal to the surface.

If there is a phase difference between ultrasonic waves reflected from different portions of a rough surface, destructive interference occurs. Therefore, the reflection of ultrasound decreases with the increase of roughness.

When the incident and the reflected waves are both normal to the surface, namely, $\theta_i = \theta_r = 0°$, Eq. (1) becomes:

$$a(f) = a_0 \exp\left[-8R_q^2\pi^2f^2/c^2\right] \tag{2}$$

where $f = kc/(2\pi)$ refers to frequency and c is the wave velocity. Furthermore, the attenuation (in dB) caused by the scattering on the rough surface is:

$$A(f) = 20 \log_{10}\left(\frac{a_0}{a(f)}\right) = \frac{160R_q^2\pi^2}{\ln(10)c^2}f^2 \tag{3}$$

Once the attenuation versus frequency data is obtained from the ultrasonic signal, curve fitting methods can be used to obtain a coefficient G that best fits the measured data with $A(f) = Gf^2$. Then, the R_q value can be reconstructed by:

$$R_q = \sqrt{\frac{\ln(10)Gc^2}{160\pi^2}} \tag{4}$$

2.2 Correction of Beam Spreading Effect

Plane waves were assumed in previous section. However, because of the limited aperture of an ultrasonic probe, the ultrasonic energy decreases while propagating due to the beam spreading effect. This introduces additional attenuation to the ultrasonic waves, which must be corrected before the reconstruction of the surface roughness. Under the assumption of a piston source, the beam spreading correction coefficient for the mth reflection from the backwall is given by [18]:

$$D^{(m)}(f) = |1 - e^{(-iq_m)}[J_0(q_m) + iJ_1(q_m)]| \tag{5}$$

where $J_{0,1}$ are the cylindrical Bessel functions. The parameter $q_m = \pi f a^2/(V_0 z_0 + mV_l h)$ depends on the transducer radius a, the distance between the transducer and the sample z_0, the thickness of the sample, the wave velocity inside the media between the transducer and the sample V_0, and the longitudinal wave velocity in the sample V_l. For example, if we use the incident wave and the first reflection from the backwall for the reconstruction, the attenuation in Eq. (3) should be calculated by the following equation instead, and Eq. (4) is then used to reconstruct R_q.

$$A(f) = 20 \log_{10}\left(\frac{a_0 D^{(1)}(f)}{a(f)D^{(0)}(f)}\right) \tag{6}$$

3   Numerical Simulation

Finite element simulations are carried out to validate this method in a noise-free environment.

3.1   Finite Element Modeling

A 2D plain strain model of a steel 10 mm × 5 mm block was established. The rough surface was on the top, with a correlation length of 200 μm and a root-mean-squared value R_q of 2–40 μm, which were controlled by an open-source codes from MySim-Labs [19]. Five hundred FEM cases with random rough profiles (Gaussian distribution) were modelled and solved using FE software Pogo [20]. Symmetrical boundary conditions were applied to simulate an infinitely wide block. Free mesh with a gradient size control was used. To capture the fine features on the rough surface, 1-μm-size-control was applied accordingly. The element size on the bottom side was 10 μm. A five-cycle Hann-windowed 10 MHz tone-burst signal was applied on nodes at the bottom of the block, and the reflected wave was received by the same nodes. Both coherent waves and diffusive waves were captured by the receivers, but only the former was extracted by averaging signals from all receiving nodes.
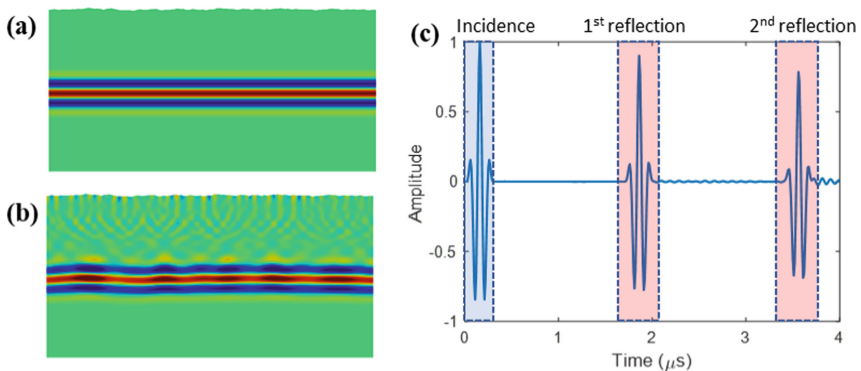

Fig. 1. FEM output when R_q = 20 μm. (a) incident wave field at t = 0.56 μs; (b) reflected wave field at t = 1.44 μs; (c) time domain coherent wave.

3.2   Simulation Results

It can be seen from Fig. 1a that a plane wave was generated, while the reflected wavefront from the rough surface was distorted, as shown in Fig. 1b. The extracted coherent signal is depicted in Fig. 1c. Clear attenuation has been observed from the backwall reflections.

The normalized spectrum of the incident wave signal and the first reflection are shown in Fig. 2a with the blue solid lines and the red dashed lines, respectively. The central frequency of the first reflection is shifted towards the lower part of the spectrum with respect to that of the incident wave, indicating stronger attenuation in the higher frequency components. The attenuation spectrum is shown in Fig. 2b. All the data points inside the −6 dB bandwidth of the first reflection, indicated by the vertical dash lines in Fig. 2a and b, are fitted by a second-order model, so that the fitted second-order coefficient G can be used to calculate R_q using Eq. (4). The R_q values are well reconstructed by the developed method, as plotted in Fig. 2c. The relative biases and the relative standard deviations have been summarized in Fig. 2d. The close-to-zero bias manifest the validity of using the phase-screen approximation to reconstruct roughness when $R_q \leq \lambda/15$, where λ is the wavelength at the central frequency. The relative standard deviations rise as the target surface becomes rougher because the phase-screen approximation becomes less accurate. Although the roughness as small as $R_q \leq \lambda/200$ can be reconstructed in the simulation, the actual sensitivity in the experiment will be compromised due to the presence of background noise and the attenuation from grain scattering.
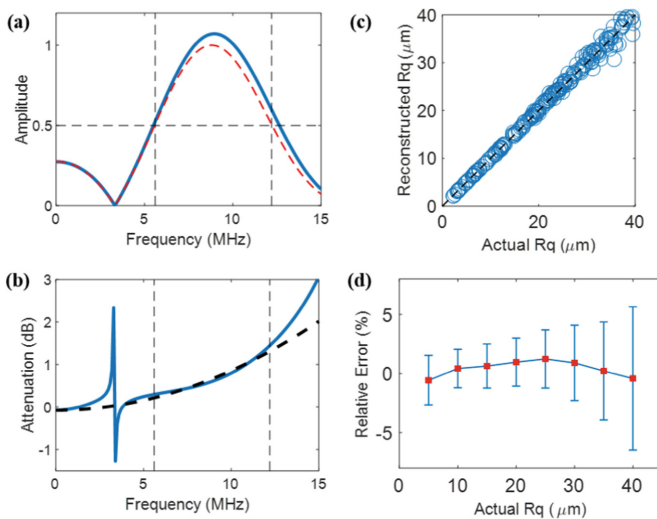
Fig. 2. Roughness reconstruction from FEM. (a) Frequency domain of the incident wave (blue solid) and the first reflection (red dash) for the case of R_q = 20 μm; (b) curve fitting of attenuation spectrum for the case of R_q = 20 μm; (c) comparison between the reconstructed and the set values; (d) relative errors.
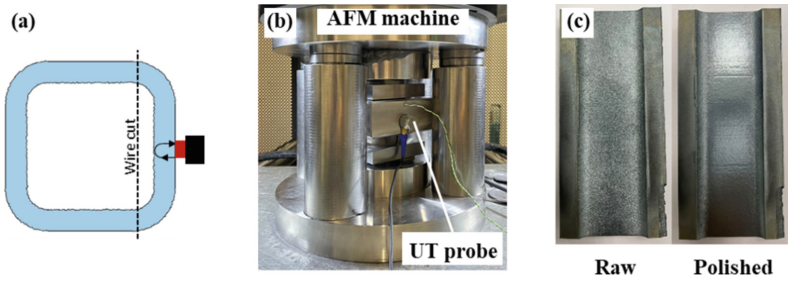
Fig. 3. Experimental validation. (a) Schematic; (b) online monitoring setup; (c) target surface before and after polishing.

4 Experimental Validation

4.1 Experimental Setup

As depicted in Fig. 3a, a square tube coupon was built using direct metal laser sintering (DMLS) of Ti64 powder. Stylus measurements on the rough surface were carried out as a reference.

A delay line transducer (Olympus, V208-RM, 20 MHz) was attached on the coupon's outer surface, as illustrated in Fig. 3b. Ultrasonic waves were generated using a pulser-receiver (LT2, Peak NDT). The coupon was then installed on an AFM machine for polishing. Pressurized abrasive media (Polyborosiloxane with 710 µm Silicon Carbide as abrasive particle) was pushed through the internal channel of the coupon upwards and downwards periodically. During this process, the roughness of the channel's surface was monitored in real-time using the proposed method.
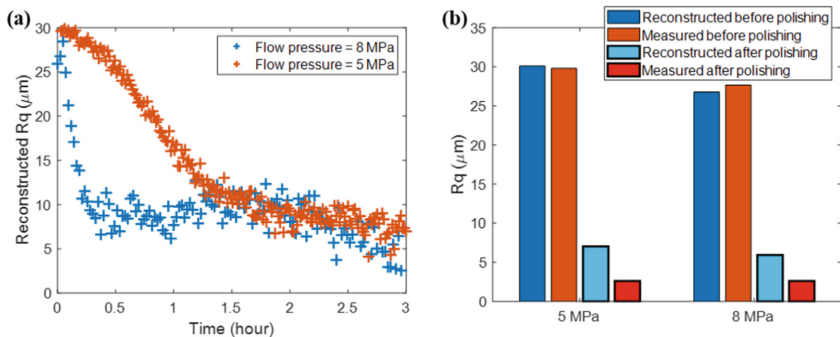
Fig. 4. Online experiment results. (a) R_q values reconstructed in real-time; (b) comparison between reconstructed R_q values and those measured by stylus profiler.

4.2   Experiment Results

The polishing work was conducted under different flow pressure: 8 MPa and 5 MPa, with each working cycle lasting for 3 h. Distinct downward trend of the reconstructed R_q values can be observed, as shown in Fig. 4a. Although it is a common sense that polishing rate increases with the flow pressure, very little quantitative guidance was established before. The reconstructed R_q value dropped from 30 μm to 10 μm in 15 min when the flow pressure was set to 8 MPa, which took 90 min under 5 MPa flow pressure. As a result, it can be concluded that a significant difference in the polishing rate (6-time difference in our case) can be achieved by tuning the pressure in an AFM process. Before and after each cycle, the roughness of the target surface was measured by a stylus profilometer for comparison. As shown in Fig. 4b, the reconstructed R_q values agree well with the measured ones for unpolished rough surface. On the other hand, the developed method suffers from the overestimation for polished surface. There are two possible reasons for this: one is that the assumption of piston source for Eq. (5) to compensate for the effect of beam spreading is not accurate enough; the other could be the contribution of intrinsic attenuation inside the propagating media become non-negligible as the target surface is getting smother.

5   Conclusions

An ultrasonic based technique is developed to monitor the surface roughness of the internal channels. A frequency-based ultrasonic method using the phase-screen approximation was used to reconstruct the roughness information of target internal surfaces. This method was first validated by FEM simulations, showing ±5% accuracy when R_q is lower than 1/15 of the ultrasonic wavelength. The technique was then applied to monitor the roughness of the internal channels during the AFM process. The reconstruction offered quantitative evaluation of the internal surface roughness in real-time. Additionally, the slope of the reconstructed roughness could be used to indicate the polishing rate, leading to the possibility for the feedback control. Slight overestimation has been observed in the experiment by comparing the reconstructed roughness and the one measured by stylus profilometer, suggesting further work is needed to improve the accuracy.

References

1. Chan, K.S., Koike, M., Mason, R.L., Okabe, T.: Fatigue life of titanium alloys fabricated by additive layer manufacturing techniques for dental implants. Metall Mater Trans A **44**(2), 1010–1022 (2013). https://doi.org/10.1007/s11661-012-1470-4
2. Vayssette, B., Saintier, N., Brugger, C., Elmay, M., Pessard, E.: Surface roughness of Ti-6Al-4V parts obtained by SLM and EBM: effect on the high cycle fatigue life. Procedia Eng. **213**, 89–97 (2018). https://doi.org/10.1016/j.proeng.2018.02.010
3. Blessing, G.V., Eitzen, D.G.: Ultrasonic measurements of surface roughness. In: Nondestructive Characterization of Materials, Saarbrücken, pp. 763–770 (1989). https://doi.org/10.1007/978-3-642-84003-6_88

4. Saniman, M.N.F., Ihara, I.: Application of air-coupled ultrasound to noncontact evaluation of paper surface roughness. J. Phys. Conf. Ser. **520**, 012016 (2014). https://doi.org/10.1088/1742-6596/520/1/012016

5. Stor-Pellinen, J., Haeggström, E., Karppinen, T., Luukkala, M.: Air-coupled ultrasonic measurement of the change in roughness of paper during wetting. Meas. Sci. Technol. **12**(8), 1336–1341 (2001). https://doi.org/10.1088/0957-0233/12/8/348

6. Stor-Pellinen, J., Luukkala, M.: Paper roughness measurement using airborne ultrasound. Sens. Actuators A **49**(1), 37–40 (1995). https://doi.org/10.1016/0924-4247(95)01011-4

7. Chimenti, D.E.: Review of air-coupled ultrasonic materials characterization. Ultrasonics **54** (7), 1804–1816 (2014). https://doi.org/10.1016/j.ultras.2014.02.006

8. Blessing, G., Slotwinski, J., Eitzen, D., Ryan, H.: Ultrasonic measurements of surface roughness. Appl. Optics **32**(19), 3433–3437 (1993). https://doi.org/10.1364/AO.32.003433

9. Smith, R.A., Bruce, D.A.: Pulsed ultrasonic spectroscopy for roughness measurement of hidden corroded surfaces. Insight Non-Destruct. Test. Cond. Monit. **43**(3), 168–172 (2001)

10. Ultrasonic spectroscopy using a rapid sweep technique. In: Presented at the 16th WCNDT 2004 - World Conference on NDT, Montreal, Canada (2004). Accessed 11 Sept 2021. https://www.ndt.net/article/wcndt2004/html/general_nde/543_buckley/543_buckley.htm

11. Sukmana, D.D., Ihara, I.: Surface roughness characterization through the use of diffuse component of scattered air-coupled ultrasound. Jpn. J. Appl. Phys. **45**(5S), 4534 (2006). https://doi.org/10.1143/JJAP.45.4534

12. Wilhjelm, J.E., Pedersen, P.C., Jacobsen, S.M.: The influence of roughness, angle, range, and transducer type on the echo signal from planar interfaces. IEEE Trans. Ultrason. Ferroelectr. Freq. Control **48**(2), 511–521 (2001). https://doi.org/10.1109/58.911734

13. Adler, R.S., et al.: Quantitative assessment of cartilage surface roughness in osteoarthritis using high frequency ultrasound. Ultrasound Med. Biol. **18**(1), 51–58 (1992). https://doi.org/10.1016/0301-5629(92)90008-X

14. Chiang, E.H., Adler, R.S., Meyer, C.R., Rubin, J.M., Dedrick, D.K., Laing, T.J.: Quantitative assessment of surface roughness using backscattered ultrasound: The effects of finite surface curvature. Ultrasound Med. Biol. **20**(2), 123–135 (1994). https://doi.org/10.1016/0301-5629(94)90077-9

15. Shi, F., Lowe, M.J.S., Craster, R.V.: Recovery of correlation function of internal random rough surfaces from diffusely scattered elastic waves. J. Mech. Phys. Solids **99**, 483–494 (2017). https://doi.org/10.1016/j.jmps.2016.11.003

16. Gunarathne, G.P.P., Christidis, K.: Measurements of surface texture using ultrasound. IEEE Trans. Instrum. Meas. **50**(5), 1144–1148 (2001). https://doi.org/10.1109/19.963174

17. Nagy, P.B., Rose, J.H.: Surface roughness and the ultrasonic detection of subsurface scatterers. J. Appl. Phys. **73**(2), 566–580 (1993). https://doi.org/10.1063/1.353366

18. Bhattacharjee, A., Pilchak, A.L., Lobkis, O.I., Foltz, J.W., Rokhlin, S.I., Williams, J.C.: Correlating ultrasonic attenuation and microtexture in a near-alpha titanium alloy. Metall. Mater. Trans. A **42**(8), 2358–2372 (2011). https://doi.org/10.1007/s11661-011-0619-x

19. Garcia, N., Stoll, E.: Monte Carlo calculation for electromagnetic-wave scattering from random rough surfaces. Phys. Rev. Lett. **52**(20), 1798–1801 (1984). https://doi.org/10.1103/PhysRevLett.52.1798

20. Huthwaite, P.: Accelerated finite element elastodynamic simulations using the GPU. J. Comput. Phys. **257**, 687–707 (2014). https://doi.org/10.1016/j.jcp.2013.10.017